High-pressure and high-temperature characteristics of a Fabry–Perot interferometer based on photonic crystal fiber

Chuang Wu,[1,2] H. Y. Fu,[1] Khurram Karim Qureshi,[3] Bai-Ou Guan,[4] and H. Y. Tam[1,*]

[1]*Photonics Research Centre, Department of Electrical Engineering, The Hong Kong Polytechnic University, Hong Kong, China*

[2]*PolyU-DUT Joint Research Center for Photonics, Dalian University of Technology, Dalian 116024, China*

[3]*Electrical Engineering Department, King Fahd University of Petroleum and Minerals, Dhahran-31261, Saudi Arabia*

[4]*Institute of Photonics Technology, Jinan University, Guangzhou 510632, China*

**Corresponding author: eehytam@polyu.edu.hk*

Received October 5, 2010; revised November 24, 2010; accepted December 8, 2010;
posted January 7, 2011 (Doc. ID 136172); published January 31, 2011

A fiber-optic Fabry–Perot interferometer was constructed by splicing a short length of photonic crystal fiber to a standard single-mode fiber. The photonic crystal fiber functions as a Fabry–Perot cavity and serves as a direct sensing probe without any additional components. Its pressure and temperature responses in the range of 0–40 MPa and 25 °C–700 °C were experimentally studied. The proposed sensor is easy to fabricate, potentially low-cost, and compact in size, which makes it very attractive for high-pressure and high-temperature sensing applications. © 2011 Optical Society of America

OCIS codes: 060.2370, 120.2230, 060.5295.

A Fabry–Pérot interferometer (FPI) consists of an optical cavity formed by two closely spaced mirrors. Multiple reflections between the mirrors introduce multiple beams that interfere with each other, resulting in an interference fringe pattern in the spectral domain. The fringe pattern can be modulated by external perturbations that induce changes in either the refractive index and/or physical length of the cavity, allowing FPIs to be used in various sensing applications [1]. Fiber-optic FPI sensors have been attracting much interest because they offer many outstanding advantages, such as high sensitivity, high-temperature survivability, compact size, corrosion resistance, and immunity to electromagnetic interference [2]. These advantages make them very suitable for deployment in space-limited harsh environments such as turbine engines and power plants and in the oil and gas industry, where pressure and temperature are the two most common measurands [3–7].

Many methods have been developed to fabricate fiber-optic FPIs. These include using conventional hollow-core fiber [3–5], chemical etching [7,8], and laser micromachining [9,10]. Recently, FPIs made from hollow-core photonic bandgap fiber [11] and solid-core photonic crystal fiber (PCF) [12] by simply cleaving and splicing have been demonstrated as strain and temperature sensors. The former needs a coating film onto the fiber endface, thereby increasing the complexity of the fabrication process. The latter as a temperature sensor is not stable, because the air holes are exposed to external environment [13].

In this Letter, we report a fiber-optic FPI constructed by splicing a solid-core PCF to a standard single-mode fiber (SMF), and the other end of the PCF was collapsed with arc discharge using a fusion splicer. The entire fabrication process was performed using a commercially available fusion splicer. The principle of the FPI sensor is also presented here. We experimentally investigated the high-pressure and high-temperature characteristics of the proposed FPI sensor. Measurements of pressure up to 40 MPa and temperature up to 700 °C were carried out. The pressure and temperature coefficients of the FPI sensor were measured to be −5.8 pm/MPa and ~13 pm/°C, respectively. The experimental results agree well with the theoretical analysis.

Figure 1(a) illustrates the experimental setup of our measurement. A broadband source (BBS) centered at 1530 nm is used to illuminate the FPI through an optical circulator. The reflection spectrum of the FPI is observed by an optical spectrum analyzer (OSA). Figures 1(b) and 1(c) show the schematic diagram and photograph of the fabricated FPI. A short length of a solid-core PCF (PM-1550-01 by Blaze Photonics) was first spliced to a standard SMF using the technique reported in [14]. Because of the small difference in refractive index between the SMF and the PCF, a mirror with relatively low reflectivity was formed at the fiber interface. The PCF was then cleaved to a length of several millimeters. A second low-reflection mirror at the end of the solid core was formed due to Frésnel reflection. As a result, a relatively weak FPI was constructed with an intensity contrast of ~6 dB as shown in Fig. 2(a). To enhance the reflectivity of the second mirror, we collapsed the air holes with arc discharge using a fusion splicer (Furukawa FITEL-S177). The intensity contrast of the FPI increased to about 14 dB after five arc discharges, and the results are shown

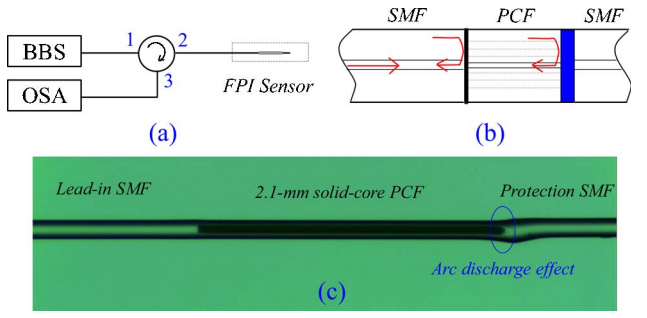

Fig. 1. (Color online) (a) Experimental setup for the measurements. (b) Schematic of the FPI sensor head. (c) Photograph of the 2.1-mm-long FPI sensor.

in Fig. 2(b). The insets of Fig. 2(a) show the side faces of the PCF before and after arc discharge. The air holes near the fiber end collapsed after arc discharges, and this helps to reflect more light back to the optical cavity, resulting in a higher reflectivity. Compared with previously reported scheme of coating film to the fiber endface to enhance reflectivity [11], our method based on arc discharge is much more simple and potentially low-cost. We can also collapse the first end of the PCF before it is fusion spliced to the SMF to increase its reflectivity; however, this leads to very high splicing loss and is thus difficult to observe the interference fringe.

The optical phase difference induced by the PCF, as shown in Fig. 1(b), can be described [1] as

$$\varphi = \frac{4\pi n_{\text{eff}} L}{\lambda}, \tag{1}$$

where n_{eff} is the effective refractive index of the fundamental mode of the PCF, L is the length of the PCF, and λ is free-space wavelength. For a certain dip in the spectrum under observation, its optical phase can be expressed by $2m\pi$ (where m is an integer). Thus, the wavelength of the dip λ_m under observation is expressed as

$$\lambda_m = \frac{2n_{\text{eff}} L}{m}. \tag{2}$$

When the FPI is subjected to external perturbations, the wavelength shift can be expressed as

$$\Delta\lambda = \left(\frac{\Delta n_{\text{eff}}}{n_{\text{eff}}} + \frac{\Delta L}{L}\right)\lambda_m = \left(\frac{\Delta n_{\text{eff}}}{n_{\text{eff}}} + \varepsilon_z\right)\lambda_m, \tag{3}$$

where Δn_{eff} and ΔL are the induced changes in n_{eff} and L, respectively, due to external perturbations, and $\varepsilon_z = \Delta L/L$ is the axial strain.

From Eq. (3), we can see that changes in n_{eff}, and axial strain in the PCF cause wavelength shift. When hydrostatic pressure is applied to the FPI, it will change n_{eff} due to photoelastic effect and introduce an axial strain in the fiber owing to the physical compression by hydrostatic pressure. Using a finite-element method [15], the pressure sensitivity of $\Delta n_{\text{eff}}/n_{\text{eff}}$ and ε_z of the PCF are simulated to be 4.22×10^{-6} MPa^{-1} and -7.97×10^{-6} MPa^{-1}, respectively. The sum value of these two terms is -3.75×10^{-6} MPa^{-1}, denoting a pressure sensitivity of −5.8 pm/MPa for the wavelength of 1550 nm. When the FPI is subjected to temperature variation, n_{eff} and L will change due to thermo-optic effect and thermal expansion and can be expressed as

$$\left(\frac{\Delta n_{\text{eff}}}{n_{\text{eff}}} + \frac{\Delta L}{L}\right)\frac{1}{\Delta T} = \delta + \alpha, \tag{4}$$

where $\delta = 8.3 \times 10^{-6}$ °C^{-1} and $\alpha = 0.55 \times 10^{-6}$ °C^{-1} [16] are the thermo-optic coefficient and thermal expansion coefficient of silica, respectively. At the wavelength of 1550 nm, the temperature sensitivity of the FPI is calculated to be 13.7 pm/°C.

To verify above theoretical analysis, we experimentally examined the pressure and temperature responses of two FPIs with cavity lengths of 1 mm and 2.1 mm. The second mirror of the FPI is sensitive to external refractive index [17] and is easily destroyed; therefore, the collapsed end of the PCF was spliced to a short length of SMF to protect the FPI, which makes it robust enough for pressure and temperature sensing. The sensors were first placed inside a high-pressure chamber filled with oil. A high-pressure compressor and a piezoelectric pressure gauge were connected to the chamber to vary the pressure applied to the sensor. The pressure was increased gradually with a step of 4 MPa in the range of 0–40 MPa. An OSA was used to measure the reflection spectrum of the FPI for each measurement point. Figure 3(a) shows the interference patterns of the 2.1-mm-long FPI at different hydrostatic pressures. The optical spectrum shifts toward shorter wavelength with pressure. A small power reduction in the reflection spectrum was also observed. Since the pressure measurement is determined by the wavelength shift of one of the minima in the reflection spectrum, power fluctuation therefore does not affect the measurement results. Figure 3(b) shows the wavelength shift as a function of applied hydrostatic pressure for the two FPIs. Their pressure sensitivities were measured to be −5.57 pm/MPa and −5.77 pm/MPa, both of which agree well with the theoretical value of −5.8 pm/MPa. It was also observed that if the PCF was spliced directly to the SMF without pretreatment by arc discharge, no interference fringes can be observed because of the low reflectivity at the interface of the PCF and SMF.

To investigate the temperature response of the two FPI sensors, we placed them inside a tube oven together with a thermocouple to monitor the temperature. The temperature was increased gradually to observe the shift of a wavelength minimum. When the temperature reached 700 °C, we kept it for half an hour and then let it cool down to room temperature. Figure 4(a) shows the wavelength shift during the heating and cooling processes. The linear fitted slopes of the two processes are

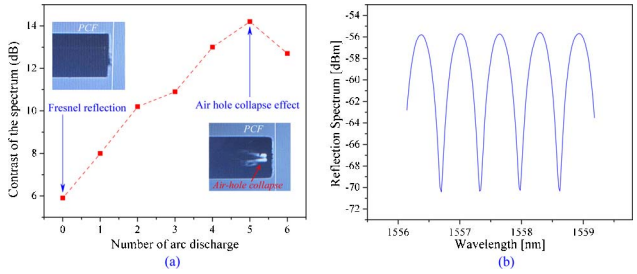

Fig. 2. (Color online) (a) Interference intensity contrast evolution versus the number of arc discharge; the insets show the photos before and after arc discharge. (b) Reflection spectrum of the 2.1-mm-long FPI after five arc discharges.

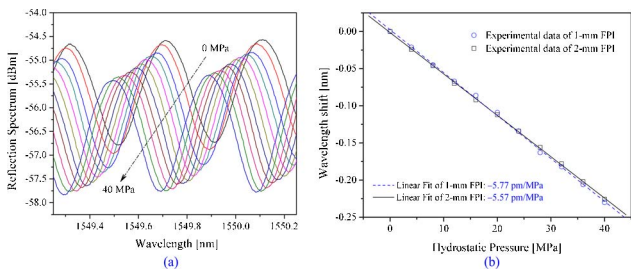

Fig. 3. (Color online) (a) Reflection spectrum of the 2.1-mm-long FPI under different applied hydrostatic pressures. (b) Wavelength shift as functions of applied hydrostatic pressure for FPIs with different cavity lengths.

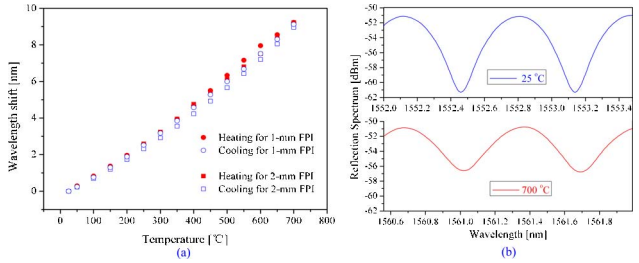

Fig. 4. (Color online) (a) Wavelength shifts as functions of applied temperature for FPIs with different cavity lengths. (b) Reflection spectrum of the 1-mm-long FPI sensor at 25 °C and at 700 °C.

13.7 pm/°C and 13.1 pm/°C for the 2.1-mm-long FPI, 14.0 pm/°C and 13.5 pm/°C for the 1 mm FPI, respectively. All of them agree well with the theoretical value of 13.7 pm/°C. The reflection spectra at 25 °C and 700 °C are shown in Fig. 4(b). A reflected power and intensity contrast reduction was also observed when the FPI was exposed to high temperature. However, it does not affect the measurement of the wavelength shift. Although the signal became weak at 700 °C, it is still very easy to obtain the wavelength shift information.

Equation (3) indicates that the sensitivity of the sensor depends on the axial strain applied to the fiber, regardless of the cavity length L. As a result, when the wavelength-tracking method is used, FPIs with different L have a constant sensitivity, as demonstrated by the experiments. Therefore, precise control of the PCF length is not required, which simplifies the production of the sensor. However, the wavelength shift overflows one period at high temperatures, which makes it difficult to determine how many periods it has shifted. In this case, a fast Fourier transform method [1] is preferred for practical use. Nevertheless, this study focuses on investigating the intrinsic pressure and temperature sensitivities of such PCF-based FPI sensors. Therefore, the interrogation method is not of as much interest in this study.

In conclusion, we reported the investigation of a PCF-based FPI fabricated by a simple fusion splicing technique and its sensing capability for high-pressure and high-temperature measurements. The experimental findings are in good agreement with the theoretical analysis. The proposed FPI is simple to fabricate, compact in size, and suitable for high-pressure and high-temperature measurements. These advantages make the proposed sensor a promising candidate for various sensing applications in harsh environments.

This work was supported by Research Grant Council General Research Fund of the Hong Kong government under project PolyU 5281/08E and by the Key Project of the National Natural Science Foundation of China (NSFC) under grant 60736039. It is also a part of the research project SB100007 funded by Saudi Basic Industries (SABIC) of Saudi Arabia.

References

1. H. F. Taylor, in *Fiber Optic Sensors*, F. T. S. Yu and S. Yin, eds. (Dekker, 2002), pp. 41–74.
2. Y. J. Rao, Opt. Fiber Technol. **12**, 227 (2006).
3. X. Wang, J. Xu, Y. Zhu, K. L. Cooper, and A. Wang, Opt. Lett. **31**, 885 (2006).
4. J. Xu, X. Wang, K. L. Cooper, G. R. Pickrell, and A. Wang, IEEE Photonics Technol. Lett. **18**, 1134 (2006).
5. H. Y. Choi, K. S. Park, S. J. Park, U. C. Paek, B. H. Lee, and E. S. Choi, Opt. Lett. **33**, 2455 (2008).
6. C. M. Jewart, Q. Wang, J. Canning, D. Grobnic, S. J. Mihailov, and K. P. Chen, Opt. Lett. **35**, 1443 (2010).
7. Y. Zhu, K. L. Cooper, G. R. Pickrell, and A. Wang, J. Lightwave Technol. **24**, 861 (2006).
8. X. Chen, F. Shen, Z. Wang, Z. Huang, and A. Wang, Appl. Opt. **45**, 7760 (2006).
9. S. Watson, M. J. Gander, W. N. MacPherson, J. S. Barton, J. D. C. Jones, T. Klotzbuecher, T. Braune, J. Ott, and F. Schmitz, Appl. Opt. **45**, 5590 (2006).
10. Z. L. Ran, Y. J. Rao, H. Y. Deng, and X. Liao, Opt. Lett. **32**, 3071 (2007).
11. Y. J. Rao, T. Zhu, X. C. Yang, and D. W. Duan, Opt. Lett. **32**, 2662 (2007).
12. J. Villatoro, V. Finazzi, G. Coviello, and V. Pruneri, Opt. Lett. **34**, 2441 (2009).
13. J. Villatoro, M. P. Kreuzer, R. Jha, V. P. Minkovich, V. Finazzi, G. Badenes, and V. Pruneri, Opt. Express **17**, 1447 (2009).
14. M. L. V. Tse, H. Y. Tam, L. B. Fu, B. K. Thomas, L. Dong, C. Lu, and P. K. A. Wai, IEEE Photonics Technol. Lett. **21**, 164 (2009).
15. C. Wu, B. O. Guan, Z. Wang, and X. Feng, J. Lightwave Technol. **28**, 1392 (2010).
16. S. Takahashi and S. Shibata, J. Non-Cryst. Solids **30**, 359 (1979).
17. J. R. Zhao, X. G. Huang, W. X. He, and J. H. Chen, J. Lightwave Technol. **28**, 2799 (2010).